ELSEVIER

Remote Sensing of Environment 80 (2002) 47–54

Remote Sensing of Environment

www.elsevier.com/locate/rse

Estimate of noise and systematic error in early thermal infrared data of the Moderate Resolution Imaging Spectroradiometer (MODIS)

Zhengming Wan*

Institute for Computational Earth System Science, University of California, Santa Barbara, CA 93106 USA

Received 18 December 2000; received in revised form 13 June 2001; accepted 15 June 2001

Abstract

The present article is a study of the channel-dependent noise and systematic error in Moderate Resolution Imaging Spectroradiometer (MODIS) thermal infrared (TIR) data in bands 20–25 and 27–36 using early MODIS data over lake and ocean sites in clear-sky days acquired with the A-side of scan mirror and electronics before the end of October 2000. In 14 cases of subarea sites with a size of 10 lines by 16 pixels each line, where the brightness temperature in band 31 changes within ±0.1 K, average and standard deviation values of brightness temperatures in 10 channels (consisting a 10-element linear detector array) of 16 MODIS TIR bands show the channel-dependent noise and systematic errors. A method is presented to separate the channel-dependent systematic error from noise due to variations in surface and atmospheric conditions. This case study shows that in the total 160 MODIS TIR channels, three channels are too noisy to use, 10 channels have significant channel-dependent noise, and all other channels met the specification of noise equivalent temperature difference (NEDT). After correcting the channel-dependent systematic errors, the quality of the MODIS TIR data is significantly improved in bands 22–25 and 27–30. More uniform sites in the brightness temperatures of bands 33–36 are needed to accurately estimate the values of channel-dependent systematic errors because the effects of spatial variations in atmospheric conditions are often larger in these four bands.

1. Introduction

The Moderate Resolution Imaging Spectroradiometer (MODIS) was developed as the keystone instrument (Salomonson, Barnes, Maymon, Montgomery, & Ostrow, 1989) on the Earth Observing System (EOS) AM-1 (also named Terra) and EOS PM ("Aqua") platforms (King, Herring, & Diner, 1995) for global studies of atmosphere, land, and ocean processes (Esaias et al., 1998; Justice et al., 1998; King, Kaufman, Menzel, & Tanré, 1992). The MODIS instrument scans ±55° from nadir in 36 bands, with bands 1–19 and 26 in the visible and near infrared range. The remaining 16 bands are in the thermal infrared (TIR) from 3 to 15 μm all at a nadir geometric instantaneous field-of-view of 1 km. The noise equivalent temperature difference (NEDT) specification of MODIS TIR bands are given in Table 1. Barnes, Pagano, and Salomonson (1998) described the prelaunch characteristics of the MODIS Proto-Flight Model (PFM), including relative spectral response (RSR) profiles and NEDT values measured in the vacuum chamber. The measured NEDT values meet the specified requirements in most bands except band 36 and channel 8 of band 35. More details are available at the MODIS Calibration Support Team (MCST) home page (mcstweb.gsfc.nasa.gov/Home.html).

The MODIS was successfully launched from Vandenberg Air Force Base, California on December 18, 1999. The MODIS-calibrated radiance daily level-1B data product (MOD02) and other products are available at the EOS Data Gateway (http://redhook.gsfc.nasa.gov/~imswww/pub/imswelcome).

The performance of the MODIS instrument may be affected by any potential small change in the optical status of instrument caused in the rapid launch process and in the long period of postlaunch instrument outgases in the orbit. It was observed that there are persistent interline noise patterns in several TIR band images, and occasionally, there are missing lines in some bands. Therefore, it is important to have the knowledge of the systematic error and noise in the MODIS level-1B radiance data (Guenther et al., 1998) during the normal MODIS Earth View operation in the

* Tel.: +1-805-893-4541; fax: +1-805-893-2578.
E-mail address: wan@icess.ucsb.edu (Z. Wan).

0034-4257/01/$ – see front matter
PII: S0034-4257(01)00266-8

Table 1
The NEDT specification of the EOS MODIS bands

Band no.	Bandwidth (μm)	IFOV (km)	NEDT (K)
20	3.660–3.840	1	0.05
21	3.929–3.989	1	2.00
22	3.929–3.989	1	0.07
23	4.020–4.080	1	0.07
24	4.433–4.498	1	0.25
25	4.482–4.549	1	0.25
27	6.535–6.895	1	0.25
28	7.175–7.475	1	0.25
29	8.400–8.700	1	0.05
30	9.580–9.880	1	0.25
31	10.780–11.280	1	0.05
32	11.770–12.270	1	0.05
33	13.185–13.485	1	0.25
34	13.485–13.785	1	0.25
35	13.785–14.085	1	0.25
36	14.085–14.385	1	0.35

orbit before evaluating the calibration accuracy of MODIS TIR data and using the MODIS TIR data in quantitative applications such as retrieving landsurface temperature (Wan & Dozier, 1996; Wan & Li, 1997), sea surface temperature (SST), and atmospheric temperature and water vapor profiles.

This study will focus on noise analysis of the early MODIS TIR data acquired with the A-side of scan mirror and electronics before the end of October 2000.

2. Approach

In order to estimate the channel-dependent systematic error and noise during the normal MODIS Earth View operation in the orbit, it is crucial to find some subarea sites where the surface and atmospheric conditions are as uniform as possible. The sensitivities of the MODIS band brightness temperatures on the variations in surface and atmospheric conditions are calculated with the state-of-the-art atmospheric radiative transfer model MODTRAN4.0 (Berk et al., 1999) and are shown in Table 2. The atmospheric temperature and water vapor profile measured by radiosonde at the shore of Lake Titicaca is used as the baseline profile in the MODTRAN calculations. Only simple shifting and scaling are used to describe the variations in atmospheric temperature, water vapor, and molecular densities in the sensitivity study. The numbers in Table 2 will change with baseline atmospheric profile, different ways in which the atmospheric temperature, and water vapor profiles changes (for example, changes only at certain levels). However, Table 2 is enough to show that the atmospheric effects are small in band 31. The prelaunch characteristics of the MODIS instrument indicates that band 31 is the best-performance band. Therefore, we can search for uniform subarea sites with the MODIS data in band 31. The size of the subarea sites cannot be too small. There are at least 10 lines and 10 pixels each line in the subarea sites so that we can investigate each channel. The size of subareas also cannot be too large because the variations in surface and atmospheric conditions become larger as the size increases. After trial and error, we find that a size of 10 lines by 16 pixels each line is reasonable. One can get a meaningful statistical value for each channel from averaging in 16 pixels.

Large lakes are good candidates for the uniform subarea sites because the surface temperature in the middle of large lakes only changes by a few degree, especially in convectively mixed periods (Malm & Jönsson, 1994). Oceans are also good candidates for the uniform subarea sites. So far, 14 cases of uniform subarea sites with a size of 10 lines by 16 pixels each line have been found. Information on these sites is shown in Table 3. In all these sites over Lake Titicaca, Great Lakes, Gulf of Mexico, and over oceans, the brightness temperature in band 31 changes within ±0.1 K, i.e., ±2 × NEDT. The MODIS data in these cases are acquired with the A-side of scan mirror and electronics before the end of October 2000.

In such selected sites, the pixel brightness temperature can be expressed as

$$T_k(b,c,j) = T_{k,\mathrm{asa}}(b) + \delta T_{\mathrm{sys}}(b,c) + \delta T_{k,\mathrm{noise}}(b,c,j) + \delta T_{k,\mathrm{s-a}}(b,c,j), \quad (1)$$

where case number $k=1-14$, band number $b=20-25$ and $27-36$, channel number $c=1-10$, and $j=1-16$ is the sample number during one scan. $T_{k,\mathrm{asa}}$ (b) is the accurate

Table 2
Sensitivities of the calculated MODIS TIR band brightness temperatures on the variations in surface temperature (T_s) and atmospheric parameters including temperature (T_a), water vapor (wv), carbon dioxide (CO_2) and ozone (O_3) densities, and the root of sum squares (RSS) of the sensitivities

Band no.	Center wavelength (μm)	δT_s 0.1 (K)	δT_a 0.25 (K)	δwv 5%	δCO_2 5 ppm	δO_3 −3%	RSS (K)
20	3.750	0.09	0.01	0.01			0.09
21 and 22	3.959	0.10	0.01				0.10
23	4.059	0.09	0.02		−0.01		0.09
24	4.465	0.03	0.13		−0.05		0.14
25	4.515	0.06	0.08	0.01	−0.01	0.01	0.10
27	6.715		0.24	0.35			0.42
28	7.925	0.02	0.19	0.24			0.31
29	8.550	0.09	0.02	0.03		0.01	0.10
30	9.730	0.06	0.09	0.01		0.28	0.30
31	11.03	0.10	0.01	0.02			0.10
32	12.02	0.10	0.01	0.02			0.10
33	13.335	0.06	0.09	0.02	−0.10	0.02	0.15
34	13.635	0.03	0.14	0.01	−0.14	0.02	0.20
35	13.935	0.02	0.17	0.01	−0.13	0.02	0.22
36	14.235		0.20	0.01	−0.14		0.24

The atmospheric temperature and water vapor profile measured by radiosonde on shore of Lake Titicaca on June 15, 2000 is used as the baseline profile.

Table 3
Information on the 14 cases of subarea (10 lines by 16 pixels each line) sites where MODIS TIR data are used in this study

Case no.	Date (mm/dd)	Granule ID	Starting		Center		Band 31		Site location
			Line no.	Sample no.	Latitude (°)	Longitude (°)	T_b (K)	σT_b (K)	
1	05/24	A2000145.0330	1252	636	−15.889	−69.337	285.50±0.08	0.041	Lake Titicaca
2	06/03	A2000155.1500	967	397	−16.113	−69.295	285.24±0.09	0.039	Lake Titicaca
3	06/15	A2000167.1525	470	972	−15.702	−69.522	284.64±0.07	0.034	Lake Titicaca
4	06/23	A2000175.0345	133	355	−15.510	−69.688	284.11±0.09	0.043	Lake Titicaca
5	09/30	A2000274.1505	714	540	−15.947	−69.306	284.14±0.09	0.036	Lake Titicaca
6	07/24	A2000206.0835	1833	438	45.911	36.571	293.67±0.10	0.040	Sea of Azov
7	07/27	A2000209.1040	1548	289	65.377	4.996	284.77±0.08	0.036	Ocean by Norway
8	08/01	A2000214.2040	1417	1114	67.714	−4.744	280.19±0.10	0.047	Sea near Iceland
9	08/03	A2000216.1045	936	996	70.060	33.597	281.56±0.10	0.047	Barents Sea
10	08/05	A2000218.1035	1738	991	56.556	19.902	287.64±0.09	0.051	Baltic Sea
11	08/21	A2000234.1035	1988	446	57.803	10.214	286.74±0.09	0.041	Atlantic by UK
12	08/26	A2000239.1055	1705	646	54.898	7.649	288.64±0.08	0.040	North Sea
13	09/17	A2000261.1700	419	636	42.263	−87.194	290.68±0.08	0.037	Great Lakes
14	10/12	A2000286.1655	1020	570	29.342	−87.456	296.87±0.11	0.048	Gulf of Mexico

The brightness temperature (T_b) and its standard deviation (σT_b) values in band 31 in these sites are also given.

band brightness temperature at the averaged surface and atmospheric conditions if there are no channel-dependent error and noise and no change in the surface and atmospheric conditions in the subarea. $\delta T_{\text{sys}}(b,c)$ is the channel-dependent systematic error. $\delta T_{k,\text{noise}}(b,c,j)$ is the channel-dependent noise. $\delta T_{k,\text{s-a}}(b,c,j)$ is the effect of the variations in surface and atmospheric conditions.

After averaging on 16 pixels, $\delta T_{k,\text{noise}}(b,c,j)$ should be canceled out or it is much smaller than other terms, so the average brightness temperature value in each channel becomes

$$\overline{T_k}(b,c) = \frac{1}{16}\sum_{j=1}^{16} T_k(b,c,j) = T_{k,\text{asa}}(b) + \delta T_{\text{sys}}(b,c) + \overline{\delta T_{k,\text{s-a}}}(b,c). \quad (2)$$

After averaging on channels, the last term in the above equation will be canceled out, so the band average value is (shown in Eq. (3))

$$\overline{T_k}(b) = \frac{1}{10}\sum_{c=1}^{10}\overline{T_k}(b,c) = T_{k,\text{asa}}(b) + \frac{1}{10}\sum_{c=1}^{10}\delta T_{\text{sys}}(b,c) = T_{k,\text{asa}}(b) + \overline{\delta T_{\text{sys}}}(b). \quad (3)$$

The difference between the averaged channel and band brightness temperatures is (shown in Eq. (4))

$$\overline{T_k}(b,c) - \overline{T_k}(b) = \delta T_{\text{sys}}(b,c) - \overline{\delta T_{\text{sys}}}(b) + \overline{\delta T_{k,\text{s-a}}}(b,c). \quad (4)$$

As shown in Table 4, the brightness temperature in band 31 all changes within ±0.1 K and its standard deviation does not exceed 0.05 K in each of the 14 cases. However, the standard deviations in other bands may be larger and more variable. For each band, we sort the 14 cases in an increasing order of the standard deviation in this band. Then, the average value of the differences between the averaged channel and band brightness temperatures in the first N cases is (shown in Eq. (5))

$$\mathrm{d}T_N(b,c) = \frac{1}{N}\sum_{k=1}^{N}(\overline{T_k}(b,c) - \overline{T_k}(b)) = \delta T_{\text{sys}}(b,c) - \overline{\delta T_{\text{sys}}}(b) + \frac{1}{N}\sum_{k=1}^{N}\overline{\delta T_{k,\text{s-a}}}(b,c). \quad (5)$$

Because the effects of the variations in surface and atmospheric conditions are only parts of the overall standard deviation of the brightness temperatures in each band, they should be smaller than the standard deviation. It is more likely to cancel them out in the average with the first N cases. If they cannot be canceled out, the averaged effect of the variations in surface and atmospheric conditions becomes smaller. The term $\overline{\delta T_{\text{sys}}}(b)$ essentially is the calibration error in band b. It will be estimated in a separate paper with in situ measurement data in a vicarious field campaign (Wan et al., 2001). In this study, the focus is on the channel-dependent systematic error and noise. For this purpose, we can combined this term into the first item in Eq. (1), i.e., the $T_{k,\text{asa}}$ term. Therefore, the systematic error may be estimated by

$$\delta T_{\text{sys}}(b,c) = \mathrm{d}T_N(b,c) - \frac{1}{N}\sum_{k=1}^{N}\overline{\delta T_{k,\text{s-a}}}(b,c). \quad (6)$$

as long as

$$\frac{1}{N}\sum_{k=1}^{N}\overline{\delta T_{k,\text{s-a}}}(b,c) \ll \mathrm{d}T_N(b,c). \quad (7)$$

If the surface and atmospheric conditions vary randomly in both along and cross track directions in the 10 by 16 pixels

Table 4
Comparison between the NEDT and standard deviation (σT_b) values of MODIS TIR band brightness temperatures in 14 cases of subarea (10 lines by 16 pixels each line) sites where MODIS TIR data are used in this study

		Band no.															
Case no.	σT_b/NEDT	20	21	22	23	24	25	27	28	29	30	31	32	33	34	35	36
1	σT_b (K)	0.06	1.13	0.12	0.10	0.28	0.26	0.21	0.10	0.09	0.24	0.04	0.06	0.57	0.43	0.41	0.69
2	σT_b (K)	0.10	0.99	0.08	0.09	0.46	0.41	0.18	0.37	0.09	0.26	0.04	0.06	0.36	0.58	0.43	0.64
3	σT_b (K)	0.09	1.21	0.08	0.09	0.22	0.26	0.38	0.31	0.10	0.25	0.03	0.06	0.31	0.42	0.39	0.74
4	σT_b (K)	0.06	1.08	0.11	0.11	0.18	0.23	0.30	0.25	0.10	0.23	0.04	0.06	0.16	0.30	0.37	0.46
5	σT_b (K)	0.21	1.64	0.15	0.14	0.18	0.31	0.47	0.34	0.08	0.58	0.04	0.06	0.49	0.89	0.23	0.45
6	σT_b (K)	0.07	0.81	0.10	0.13	0.29	0.25	0.31	0.28	0.14	0.37	0.04	0.07	0.21	0.27	0.44	0.69
7	σT_b (K)	0.06	1.10	0.10	0.09	0.26	0.23	0.23	0.25	0.12	0.33	0.04	0.05	0.22	0.53	0.46	0.59
8	σT_b (K)	0.07	1.34	0.10	0.11	0.30	1.88	0.49	0.28	0.16	0.21	0.04	0.06	0.18	0.80	0.47	0.53
9	σT_b (K)	0.07	1.20	0.10	0.11	0.19	0.25	0.39	0.42	0.13	0.28	0.05	0.07	0.20	0.52	0.38	0.57
10	σT_b (K)	0.17	1.00	0.12	0.13	0.33	0.40	0.41	0.21	0.12	0.42	0.05	0.07	0.66	0.37	0.45	0.70
11	σT_b (K)	0.07	1.25	0.10	0.15	0.55	0.39	0.91	0.77	0.12	0.43	0.04	0.07	0.37	0.54	0.29	0.50
12	σT_b (K)	0.15	1.06	0.09	0.11	0.23	1.05	0.87	0.81	0.11	0.39	0.04	0.05	0.67	0.43	0.34	0.61
13	σT_b (K)	0.12	0.89	0.09	0.11	0.37	0.28	0.95	0.61	0.11	0.61	0.04	0.06	0.21	0.59	0.28	0.47
14	σT_b (K)	0.11	1.02	0.12	0.12	0.34	0.29	0.91	0.61	0.12	0.41	0.05	0.07	0.49	0.34	0.28	0.58
Minimum	σT_b (K)	0.06	0.81	0.08	0.09	0.18	0.23	0.18	0.10	0.09	0.21	0.03	0.05	0.16	0.27	0.23	0.45
Specification	NEDT (K)	0.05	2.0	0.07	0.07	0.25	0.25	0.25	0.25	0.05	0.25	0.05	0.05	0.25	0.25	0.25	0.35

The three noisy channels were excluded.

subarea sites, the averaged effect of spatial variations in surface and atmospheric conditions will be

$$\frac{1}{N}\sum_{k=1}^{N}\overline{\delta T_{k,s-a}}(b,c) \le \frac{1}{4\sqrt{N}}\sigma T_b, \tag{8}$$

where σT_b is the average standard deviation in band b in the first N cases and factor 4 comes from the channel averaging on 16 pixels (Eq. (8)).

3. Results

After the calculation of average brightness temperature value in each channel, $\overline{T_k}(b,c)$, the standard deviation, σT_k (b,c), is calculated for all bands in the 14 cases. It is found that the ninth channel in bands 21 and 24 and the fourth channel in band 22 are too noisy to use. For all other channels, the minimal values of σT_k (b,c) in its best cases are shown in Fig. 1. Because all the minimal σT_k (b,c) values

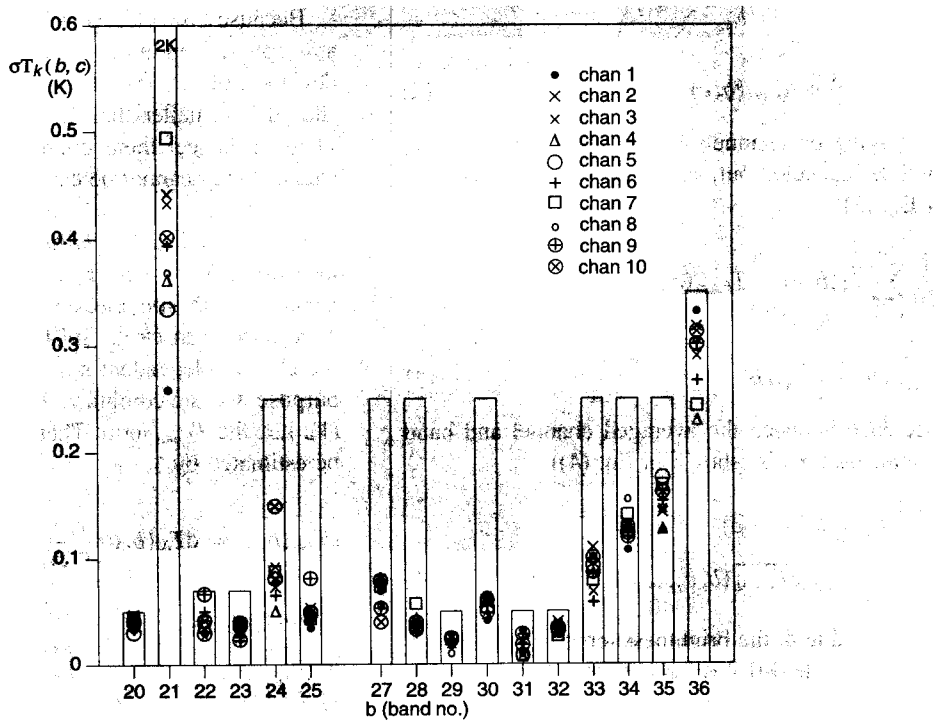

Fig. 1. The standard deviation in MODIS TIR channel brightness temperatures in its best cases of the 14 cases in this study. Note that three noisy channels were excluded.

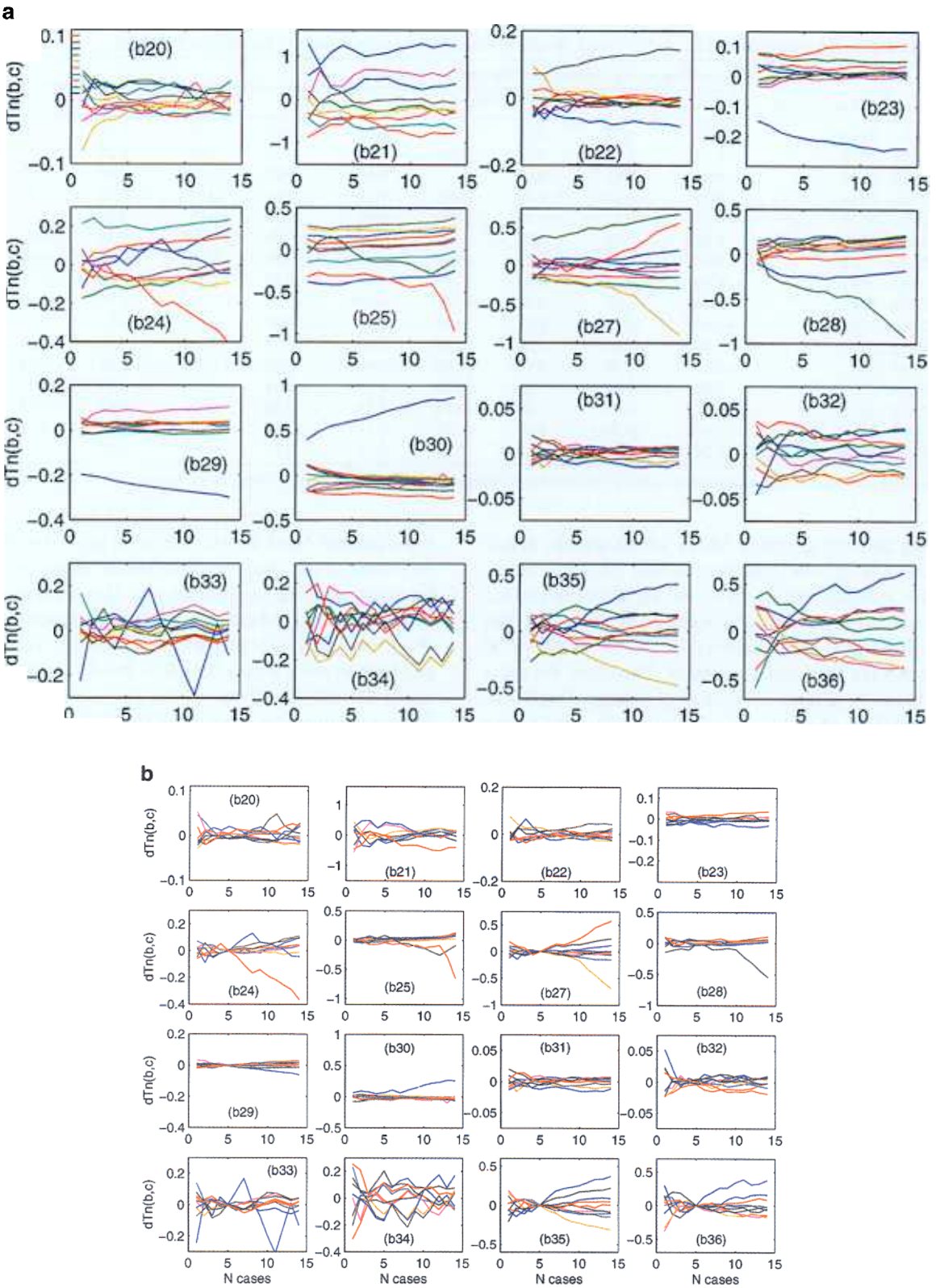

Fig. 2. The average value of the differences between the averaged channel and band brightness temperatures in N cases, $dT_N(b,c)$, vs. N. The 16 subplots in the upper half represent the results before the channel-dependent systematic error correction, and the 16 subplots in the lower half represent the results after the correction.

Table 5
The temperature difference values (in unit K) used to correct the channel-dependent systematic errors in the MODIS TIR bands

Band	Range of scene T_b (K)	Minus channel-dependent systematic error in channel									
		1	2	3	4	5	6	7	8	9	10
20	281.0–299.4	−0.01	0.02	0.01	−0.00	−0.03	−0.03	0.01	0.01	0.00	0.02
21	280.4–297.8	−1.13	0.12	0.41	0.62	−0.56	0.39	0.05	−0.28		0.38
22	280.6–297.9	0.06*	0.01	−0.01		0.02	−0.02	−0.10*	0.01	0.03	0.01
23	278.5–295.0	0.21*	−0.06	−0.03	−0.02	0.01	−0.01	−0.01	−0.02	−0.00	−0.07*
24	247.2–257.4	−0.09	0.12	−0.10	−0.20	0.05	0.08	0.09	0.00		0.05
25	262.2–276.3	0.38*	−0.03	−0.09	0.12	−0.03	−0.24	−0.28*	−0.16	0.03	0.31*
27	238.8–256.3	−0.03	0.22	0.13	−0.01	0.02	0.20	−0.02	−0.09	−0.44*	0.01
28	253.4–269.1	0.24	0.38*	0.05	−0.07	−0.06	−0.10	−0.13	−0.16	−0.11	−0.04
29	278.0–294.2	0.24*	−0.02	−0.01	−0.01	−0.09*	−0.03	−0.03	−0.00	0.00	−0.03
30	258.9–275.6	−0.61*	0.13	0.21	0.02	0.10	0.01	0.07	0.03	0.03	−0.00
31	280.2–296.9	0.00	0.00	0.00	0.00	0.00	0.00	0.00	0.00	0.00	0.00
32	279.4–296.2	−0.02	0.00	0.02	−0.00	0.01	0.03	0.02	−0.01	−0.02	−0.03
33	261.4–273.3	−0.02	−0.01	0.06	−0.03	−0.04	−0.01	−0.02	−0.04	0.07	0.04
34	250.4–261.0	−0.10	−0.03	−0.07	−0.04	−0.15	0.20	0.15	0.06	−0.03	0.01
35	244.1–252.8	−0.05	0.20	0.06	−0.07	0.11	0.17	−0.01	−0.06	−0.23	−0.12
36	229.2–234.0	−0.24	−0.13	0.10	0.09	0.21	0.20	0.19	−0.09	−0.19	−0.13

These values are estimated from averaging the channel-band brightness temperature difference values in five selected cases.

are smaller than the specified NEDT values and the actual noise should be smaller than the minimal σT_k (b,c) value, which also includes the effects of the variations in surface and atmospheric conditions, the actual noise is smaller than the specified NEDT in all channels of the 16 MODIS TIR bands except the three noisy channels. Therefore, the averaged noise can be ignored in the channel averaged brightness temperature $\overline{T_k}(b,c)$ in Eq. (2). Then, the dT_N (b,c) values can be calculated by following the steps in Section 4.

The values of the first term on the right side of Eq. (6), i.e., dT_N (b,c), are shown in 16 subplots in the upper half of Fig. 2. Each line represents one channel. The 10 short horizontal lines at the upper left side of the first plot show the colors used for each channel. The blue line at the bottom is for channel 1 and the red line at the top is for channel 10. The value of dT_N (b,c) becomes almost stable around $N=5$ for most channels in most bands. This indicates that the condition for a good estimate of channel-dependent systematic errors (Eq. (7)) is met for most channels. The values for all channels are within ±0.01 K in band 31 and ±0.03 K in bands 20 and 32. However, the first channel (channel 1) departs significantly from other channels in bands 21, 23, 29, and 30. Around $N=5$, the dT_N $(b,1)$ value is slightly larger than 1 K in band 21 (b21), is about −0.2 K in band 23 (which is three times its NEDT value 0.07 K), slightly less than −0.2 K in band 29 (which is four times its NEDT value 0.05 K), and is 0.61 K in band 30 (which is larger than two times its NEDT value 0.25 K). These numbers indicate

Table 6
Comparison between the NEDT and standard deviation (σT_b) values of MODIS TIR band brightness temperatures after the channel-dependent correction in 14 cases of subarea (10 lines by 16 pixels each line) sites where MODIS TIR data are used in this study

Case no.	σT_b / NEDT	Band no.															
		20	21	22	23	24	25	27	28	29	30	31	32	33	34	35	36
1	σT_b (K)	0.06	0.92	0.10	0.06	0.25	0.18	0.12	0.18	0.03	0.08	0.04	0.06	0.57	0.39	0.41	0.59
2	σT_b (K)	0.10	0.91	0.07	0.07	0.45	0.36	0.15	0.35	0.05	0.09	0.04	0.05	0.37	0.55	0.38	0.57
3	σT_b (K)	0.09	1.04	0.08	0.06	0.20	0.20	0.26	0.22	0.04	0.10	0.03	0.05	0.30	0.36	0.40	0.66
4	σT_b (K)	0.06	0.90	0.11	0.06	0.18	0.14	0.22	0.16	0.04	0.11	0.04	0.06	0.16	0.27	0.36	0.44
5	σT_b (K)	0.21	1.38	0.15	0.13	0.13	0.20	0.39	0.22	0.05	0.53	0.04	0.06	0.50	0.97	0.23	0.45
6	σT_b (K)	0.07	0.64	0.08	0.07	0.26	0.10	0.22	0.19	0.08	0.18	0.04	0.07	0.20	0.29	0.40	0.60
7	σT_b (K)	0.06	0.90	0.08	0.05	0.25	0.08	0.15	0.12	0.05	0.14	0.04	0.05	0.21	0.45	0.46	0.54
8	σT_b (K)	0.06	1.17	0.09	0.07	0.29	1.79	0.37	0.18	0.08	0.15	0.04	0.05	0.17	0.71	0.42	0.48
9	σT_b (K)	0.07	1.07	0.09	0.07	0.18	0.14	0.36	0.35	0.07	0.13	0.05	0.07	0.20	0.60	0.35	0.50
10	σT_b (K)	0.17	0.82	0.11	0.09	0.31	0.32	0.29	0.09	0.05	0.24	0.05	0.06	0.66	0.41	0.40	0.51
11	σT_b (K)	0.07	1.20	0.08	0.12	0.52	0.26	0.82	0.64	0.06	0.25	0.04	0.07	0.38	0.46	0.25	0.41
12	σT_b (K)	0.15	0.90	0.08	0.08	0.18	0.94	0.77	0.68	0.05	0.21	0.04	0.05	0.68	0.51	0.28	0.61
13	σT_b (K)	0.13	0.71	0.08	0.06	0.34	0.15	0.86	0.47	0.05	0.48	0.04	0.06	0.20	0.67	0.25	0.46
14	σT_b (K)	0.11	0.80	0.09	0.07	0.29	0.13	0.82	0.48	0.06	0.28	0.05	0.07	0.50	0.29	0.25	0.51
Minimum	σT_b (K)	0.06	0.64	0.07	0.05	0.13	0.08	0.12	0.09	0.03	0.08	0.03	0.05	0.16	0.27	0.23	0.41
Specification	NEDT (K)	0.05	2.0	0.07	0.07	0.25	0.25	0.25	0.25	0.05	0.25	0.05	0.05	0.25	0.25	0.25	0.35

The three noisy channels were excluded.

the necessity for the correction of the channel-dependent systematic errors in the MODIS TIR data. The minus dT_N (b,c) values at $N=5$ are given in Table 5. Although there are two lines in red, two in green, and two in blue, in Fig. 2, the channel number of key channels can be identified by a combined use of Fig. 2 and Table 5. No more point symbols are used in Fig. 2 for clarity and for the small size of subplots so that 32 subplots can be placed in a single page for easy comparison. The values in Table 5 can be used for the systematic error correction. Note that the values for band 31 are set to zero because they are within ±0.01 K, only a fifth of the NEDT value 0.05 K. After applying the correction, the standard deviations in MODIS TIR band brightness temperatures in the 14 cases are shown in Table 6. Comparing the results in Table 6 to those in Table 4 shows significant improvements made in the corrected MODIS TIR data in all bands, except bands 20 and 31–36, because the systematic error is small in bands 20 and 31–32 and the effects of spatial variations in atmospheric conditions are larger in bands 33–36. This is also clearly shown in the lower half of Fig. 2, where almost all lines get closer and vary within a fraction of ± the specified NEDT values except in bands 33–36. In these four bands, there is no significant difference made by the correction. We also tried to use dT_N (b,c) values at a larger N value (e.g., 8) in the correction but cannot get improvements in these four bands. By comparing Tables 4 and 6, we can see that the order of standard deviations in band brightness temperatures changed after the correction. This is an indication that the effects of the variations in atmospheric conditions are too large to cancel out by averaging. By comparing the standard deviations in band brightness temperatures, σT_b, shown in Table 6, to the standard deviations in channel brightness temperatures, σT_k (b,c), in Fig. 1, we can see that σT_b is larger than σT_k (b,c) even in its best cases. This indicates that the effects of the variations in the surface and atmospheric conditions are larger in σT_b, because the spatial variations in the surface and atmospheric conditions in the channel brightness temperatures only include those in the scanning direction while the spatial variations in the band brightness temperatures also include those in the along-track direction.

We expect that the channel-dependent systematic errors can be better estimated if some cases with smaller atmospheric variations in bands 33–36 could be found, though we already know that the channel-dependent systematic errors are smaller than the NEDT values specified for these bands.

After the MODIS sensor was reconfigured on October 31 and November 1, 2000, MODIS is operating on the B-side for the scan mirror and electronics systems and with an improved SW/MIR focal plane bias voltage, all TIR channels (including the ninth channel in bands 21 and 24 and the fourth channel in band 22) are working (refer to http://mcstweb.gsfc.nasa.gov/Home.html for more details). We will evaluate the channel-dependent noise and systematic error in MODIS TIR data acquired after November 1, 2000 in the near future.

4. Conclusion

From early MODIS TIR data (before the end of October 2000) in 14 cases of subareas with a size of 10 lines by 16 pixels each line, where the brightness temperature in band 31 changes within ±0.1 K, it is found that the ninth channel in bands 21 and 24 and the fourth channel in band 22 are too noisy to use and that the specification of NEDT is reached in all other channels of the 16 MODIS TIR bands. There are significant channel-dependent systematic errors in one to three channels in bands 22–23, 25, and 27–30. After correcting the channel-dependent systematic errors, the quality of the MODIS TIR data is significantly improved in bands 22–25 and 27–30. More uniform sites in the brightness temperatures of bands 33–36 are needed to accurately estimate the values of their channel-dependent systematic errors because the effects of spatial variations in atmospheric conditions are often larger in these four bands.

It is advised that the pixel-by-pixel quality assessment flags in the science data set EV_1KM_Emissive_Uncert_Indexes for each TIR bands should be checked when using MODIS level-1B TIR data in Earth Sciences research and applications.

Acknowledgments

This work was supported by EOS Program contract NAS5-31370 of the National Aeronautics and Space Administration. The author would like to thank Dr. Vincent V. Salomonson for his suggestions and encouragement and two anonymous reviewers for their valuable comments. The MODIS data were generated by the Goddard DAAC and MODAPS under supports of MODIS MCST and SDDT.

References

Barnes, W. L., Pagano, T. S., & Salomonson, V. V. (1998). Prelaunch characteristics of the Moderate Resolution Imaging Spectroradiometer (MODIS) on EOS-AM1. *IEEE Transactions on Geoscience and Remote Sensing, 36* (4), 1088–1100.

Berk, A., Anderson, G. P., Bernstein, L. S., Acharya, P. K., Dothe, H., Matthew, M. W., Adler-Golden, S. M., Chetwynd, J. H. Jr., Richtmeier, S. C., Pukall, B., Allred, C. L., Jeong, L. S., & Hoke, M. L. (1999). MODTRAN4 radiative transfer modeling for atmospheric correction. *Optical Spectroscopic Techniques and Instrumentation for Atmospheric and Space Research III, Proc. SPIE vol. 3756*, 348–353.

Esaias, W. E., Abbott, M. R., Barton, I., Brown, O. W., Campbell, J. W., Carder, K. L., Clark, D. K., Evans, R. L., Hoge, F. E., Gordon, H. R., Balch, W. P., Letelier, R., & Minnett, P. J. (1998). An overview of MODIS capabilities for ocean science observations. *IEEE Transactions on Geoscience and Remote Sensing, 36* (4), 1250–1265.

Guenther, B., Godden, G. D., Xiong, X., Knight, E. J., Qiu, S.-Y., Montgomery, H., Hopkins, M. M., Khayat, M. G., & Hao, Z. (1998). Prelaunch algorithm and data format for the level 1 calibration product for the EOS-AM1 Moderate Resolution Imaging Spectroradiometer (MODIS). *IEEE Transactions on Geoscience and Remote Sensing, 36* (4), 1142–1151.

Justice, C. O., Vermote, E., Townshend, J. R. G., Defries, R., Roy, D. O., Hall, D. K., Salomonson, V. V., Privette, J. L., Riggs, G., Strahler, A., Lucht, W., Myneni, R. B., Knyazikhin, K., Running, S. W., Nemani, P. R., Wan, Z., Huete, A. R., van Leeuwen, W., Wolfe, R. E., Giglio, L., Muller, J.-P., Knyazikhin, Y., & Barnsley, M. J. (1998). The Moderate Resolution Imaging Spectroradiometer (MODIS): land remote sensing for global change research. *IEEE Transactions on Geoscience and Remote Sensing, 36*, 1228–1249.

King, M. D., Herring, D. D., & Diner, D. J. (1995). The Earth Observing System (EOS): a space-based program for assessing mankind's impact on the global environment. *Optics & Photonics News, 6*, 34–39.

King, M. D., Kaufman, Y. J., Menzel, W. P., & Tanré, D. (1992). Remote sensing of cloud, aerosol and water vapor properties from the Moderate Resolution Imaging Spectrometer (MODIS). *IEEE Transactions on Geoscience and Remote Sensing, 30* (1), 2–27.

Malm, J., & Jönsson, L. (1994). Water surface temperature characteristics and thermal bar evolution during spring in Lake Ladoga. *Remote Sensing of Environment, 48*, 332–338.

Salomonson, V., Barnes, W., Maymon, P., Montgomery, H., & Ostrow, H. (1989). MODIS: advanced facility instrument for studies of the Earth as a system. *IEEE Transactions on Geoscience and Remote Sensing, 27* (2), 145–153.

Wan, Z., & Dozier, J. (1996). A generalized split-window algorithm for retrieving land-surface temperature from space. *IEEE Transactions on Geoscience and Remote Sensing, 34* (4), 892–905.

Wan, Z., & Li, Z.-L. (1997). A physics-based algorithm for retrieving land-surface emissivity and temperature from EOS/MODIS data. *IEEE Transactions on Geoscience and Remote Sensing, 35* (4), 980–996.

Wan, Z., Zhang, Y., Li, Z.-L., Wang, R., Salomonson, V. V., Yves, A., & Bosseno, R. (2001). Preliminary estimate of calibration of the Moderate Resolution Imaging Spectroradiometer (MODIS) thermal infrared data using Lake Titicaca. *Remote Sensing of Environment*, (revised).